THE JOURNAL OF PHYSICAL CHEMISTRY C

ARTICLE

pubs.acs.org/JPCC

Role of the Exposed Pt Active Sites and BaO_2 Formation in NO_x Storage Reduction Systems: A Model Catalyst Study on BaO_x/Pt(111)

Evgeny I. Vovk,[†,‡] Emre Emmez,[†] Mehmet Erbudak,[§] Valerii I. Bukhtiyarov,[‡] and Emrah Ozensoy*[,†]

[†]Chemistry Department, Bilkent University, 06800 Bilkent, Ankara, Turkey

[‡]Boreskov Institute of Catalysis, 630090 Novosibirsk, Russian Federation

[§]Laboratorium für Festkörperphysik, ETH Zurich, CH-8093 Zurich, Switzerland

ABSTRACT:

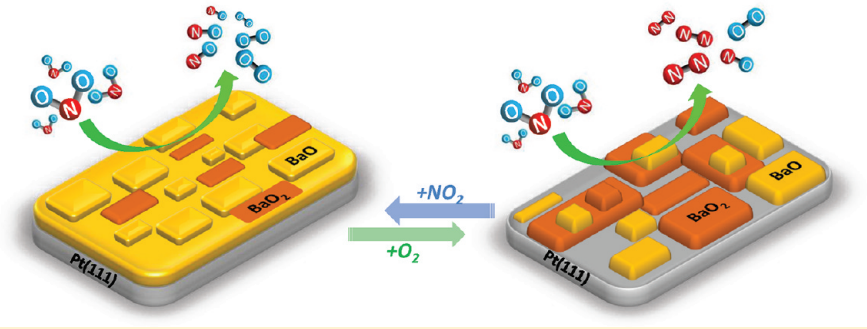

BaO_x(0.5 MLE - 10 MLE)/Pt(111) (MLE: monolayer equivalent) surfaces were synthesized as model NO_x storage reduction (NSR) catalysts. Chemical structure, surface morphology, and the nature of the adsorbed species on BaO_x/Pt(111) surfaces were studied via X-ray photoelectron spectroscopy (XPS), temperature-programmed desorption (TPD), and low-energy electron diffraction (LEED). For θ_{BaOx} < 1 MLE, (2 × 2) or (1 × 2) ordered overlayer structures were observed on Pt(111), whereas BaO(110) surface termination was detected for θ_{BaOx} = 1.5 MLE. Thicker films ($\theta_{BaOx} \geq$ 2.5 MLE) were found to be amorphous. Extensive NO_2 adsorption on BaO_x(10 MLE)/Pt(111) yields predominantly nitrate species that decompose at higher temperatures through the formation of nitrites. Nitrate decomposition occurs on BaO_x(10 MLE)/Pt(111) in two successive steps: (1) NO(g) evolution and BaO_2 formation at 650 K and (2) NO(g) + O_2(g) evolution at 700 K. O_2(g) treatment of the BaO_x(10 MLE)/Pt(111) surface at 873 K facilitates the BaO_2 formation and results in the agglomeration of BaO_x domains leading to the generation of exposed Pt(111) surface sites. BaO_2 formed on BaO_x(10 MLE)/Pt(111) is stable even after annealing at 1073 K, whereas on thinner films (θ_{BaOx} = 2.5 MLE), BaO_2 partially decomposes into BaO, indicating that small BaO_2 clusters in close proximity of the exposed Pt(111) sites are prone to decomposition. Nitrate decomposition temperature decreases monotonically from 550 to 375 K with decreasing BaO_x coverage within θ_{BaOx} = 0.5 to 1.0 MLE. Nitrate decomposition occurs at a rather constant temperature range of 650−700 K for thicker BaO_x overlayers (2.5 MLE < θ_{BaOx} < 10 MLE). These two distinctly characteristic BaO_x-coverage-dependent nitrate decomposition regimes are in very good agreement with the observation of the so-called "surface" and "bulk" barium nitrates previously reported for realistic NSR catalysts, clearly demonstrating the strong dependence of the nitrate thermal stability on the NO_x storage domain size.

1. INTRODUCTION

The reduction of NO_x emissions under the oxygen-rich exhaust environment is an important challenge faced by the automotive industry. A number of NO_x abatement technologies such as selective catalytic reduction (SCR) and three-way catalysis (TWC) have been previously developed to tackle this challenging environmental problem.[1] Another alternative after treatment DeNO$_x$ technology, is the so-called NO_x storage-reduction (NSR) catalysis introduced by Toyota Motor Company.[2−4] In this technology, during the lean operation (i.e., under oxidizing conditions) NO_x traps oxidize and store NO_x in the solid state, whereas under rich (i.e., reducing) conditions, stored NO_x is released and successively converted into harmless N_2. BaO is the most commonly utilized NO_x storage component in NSR catalysis. BaO reacts with NO_x under oxidizing conditions forming $Ba(NO_3)_2$ and $Ba(NO_2)_2$. Schmitz et al.[5] reported that on a BaO/Al_2O_3 model catalyst, BaO interacts with NO at room temperature, forming nitrite species, whereas interaction with NO_2 leads to the formation of nitrate species. It was also demonstrated in previous studies that after the introduction of NO_2 on BaO at 100 K, nitrate and nitrite species coexist on the surface.[6,7] It was also reported that nitrite species

Received: August 26, 2011
Revised: October 26, 2011
Published: October 26, 2011

possess a lower thermal stability as compared with nitrates.[8,9] In another model catalyst study on the $BaO/Al_2O_3/NiAl(110)$ surface,[10] exclusively nitrite formation was observed at 300 K during the initial stages of the NO_2 adsorption, where the nitrite species were found to be aligned parallel to the surface. With the increasing NO_2 exposure, nitrites were gradually converted into nitrates.[10] It was also reported that whereas the nitrite formation is a rapid process, conversion of nitrites into nitrates occurs at a slower pace.[10]

Formation of BaO_2 was also reported by XPS[8,10] and STM[11,12] in similar model catalyst studies. BaO_2 is a relatively stable peroxide in its bulk form, releasing oxygen at $T > 800$ K and fully decomposing at $T > 1200$ K.[13] It was suggested that in NSR applications BaO_2 formation plays an important role in the $Ba(NO_3)_2$ decomposition, where BaO_2 species generated during the nitrate decomposition exist on the surface even after the complete desorption of all of the nitrates.[7,8] Various factors influence the decomposition behavior of the stored nitrates,[14] where one of the prominent factors is the noble metal active sites (e.g., Pt) present on the NSR catalyst surface. The catalytic effect of Pt on $Ba(NO_3)_2$ decomposition has been experimentally demonstrated on $Pt/Ba/Al_2O_3$ based realistic, high surface area catalysts.[15,16] It has been shown that the Pt-catalyzed $Ba(NO_3)_2$ decomposition occurs at ~650 K, whereas in the absence of Pt sites $Ba(NO_3)_2$ starts to decompose above 750 K.[15] Despite the numerous studies on the NO_x storage mechanism of NSR systems, a fundamental molecular level understanding of this important phenomenon is still not completely established.[5,6,10,17]

The structural characterization of BaO overlayers on Cu(111) and Pt(111) surfaces have been previously discussed in former reports.[12,18,19] On the Cu(111) surface, BaO domains with (100) surface orientation were determined via LEED.[18] The (100) termination of BaO is thermodynamically more stable than other BaO surface terminations such as (110) or (111),[20] and thus, the formation of a BaO(100) overlayer structure is expected when there exists a weak interaction between the BaO overlayer and the underlying substrate, as in the case of Cu(111). On the Pt(111) surface, hexagonal BaO(111) overlayers with a (2×2) structure and an interatomic spacing of 8.1 Å were also observed via STM.[19] The stability of this (2×2) surface overlayer was also confirmed by theoretical calculations.[19]

In the current work, we focus our attention on several fundamental surface phenomena that have direct implications on the NO_x storage and release mechanisms of NSR catalysts. By utilizing well-defined model catalysts in the form of $BaO\text{-}BaO_2/Pt(111)$, we demonstrate the influence of the exposed Pt sites, Pt/BaO_x interfacial sites, variations in the BaO surface coverage on the NO_x uptake and NO_x release properties of model NSR systems. Therefore, current results provide valuable fundamental surface scientific information that shed light on the essential operational principles of realistic NSR catalysts.

2. EXPERIMENTAL SECTION

All of the experiments were performed in a custom-made multitechnique ultra high vacuum (UHV) surface analysis chamber with a base pressure of 2×10^{-10} Torr. The UHV chamber is equipped with XPS (Riber Mg/Al dual anode and Riber model EA 150 electron energy analyzer), custom-made rear-view LEED, and TPD (Dycor model DM200 M quadrupole mass spectrometer and Heatwave model 101303 PID-controlled linear sample heater) apparatus. A Pt(111) single crystal disk (10 mm diameter, 2 mm thickness, both sides atomically polished, MaTeck) was used as a substrate. The Pt(111) single crystal substrate was mounted on a Ta sample holder that can be resistively heated to 1073 K and cooled via liquid nitrogen to 80 K. The sample temperature was monitored by a K-type thermocouple (wire thickness 0.05 mm, Omega) spot-welded on the lateral edge of the crystal. The Pt(111) surface was cleaned by multiple cycles of Ar^+ (Ar(g), Linde AG, 99.999% purity) sputtering at 1.5 kV and subsequent heating at 1073 K in vacuum. The cleanness of the surface was confirmed by XPS and LEED. Typically, BaO_x layers on Pt(111) were prepared by thermal evaporation of Ba(g) from a $BaAl_4$ alloy (ST2/FR wire, SAES Getters) on a Pt(111) surface at 100 K that was precovered with NO_2/N_2O_4 multilayer and subsequent heating in vacuum to 1073 K (to remove NO_x species and fully oxidize the Ba overlayer). The utilization of a NO_2/N_2O_4 multilayer as an oxidizing agent for the preparation of BaO layers in model catalyst systems has been used in a number of former investigations.[7−9] This preparation method enables an oxidation route that can take place at relatively lower temperatures in comparison with a conventional oxidation route involving O_2 as an oxidizing agent that typically requires a higher temperature for the activation of the O−O linkages. The NO_2/N_2O_4 multilayer on Pt(111) was prepared by exposing the clean Pt(111) surface to 5×10^{-8} Torr NO_2 for 1 min at 100 K. NO_2 gas was synthesized by the reaction of NO (99.9% purity, Air Products) with O_2 (99.999% purity, Linde AG) and further purification by subsequent freeze−thaw−pump cycles. BaO film thickness on Pt(111) substrate was estimated by assuming a uniform BaO_x overlayer and by utilizing the attenuation of the Pt $4f_{7/2}$ XPS

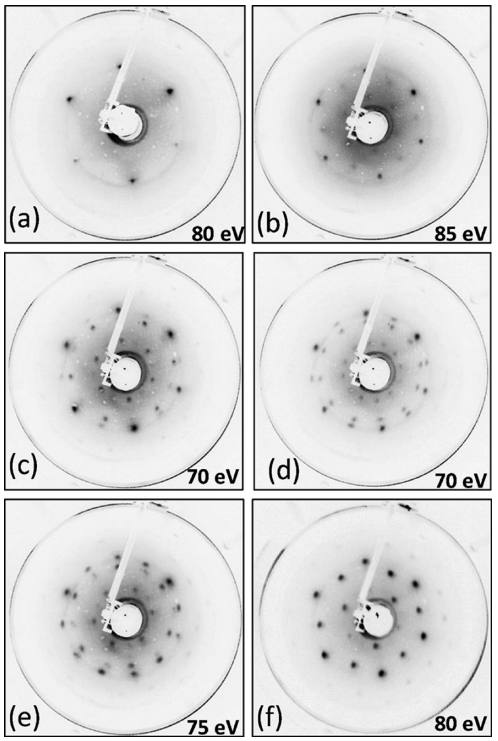

Figure 1. LEED patterns obtained in various stages of the BaO_x(0.5 MLE)/Pt(111) film preparation process. (See the text for details.) All of the LEED images were obtained at 323 K. Electron energy values used during the data acquisition are also provided in the right bottom corner of each image.

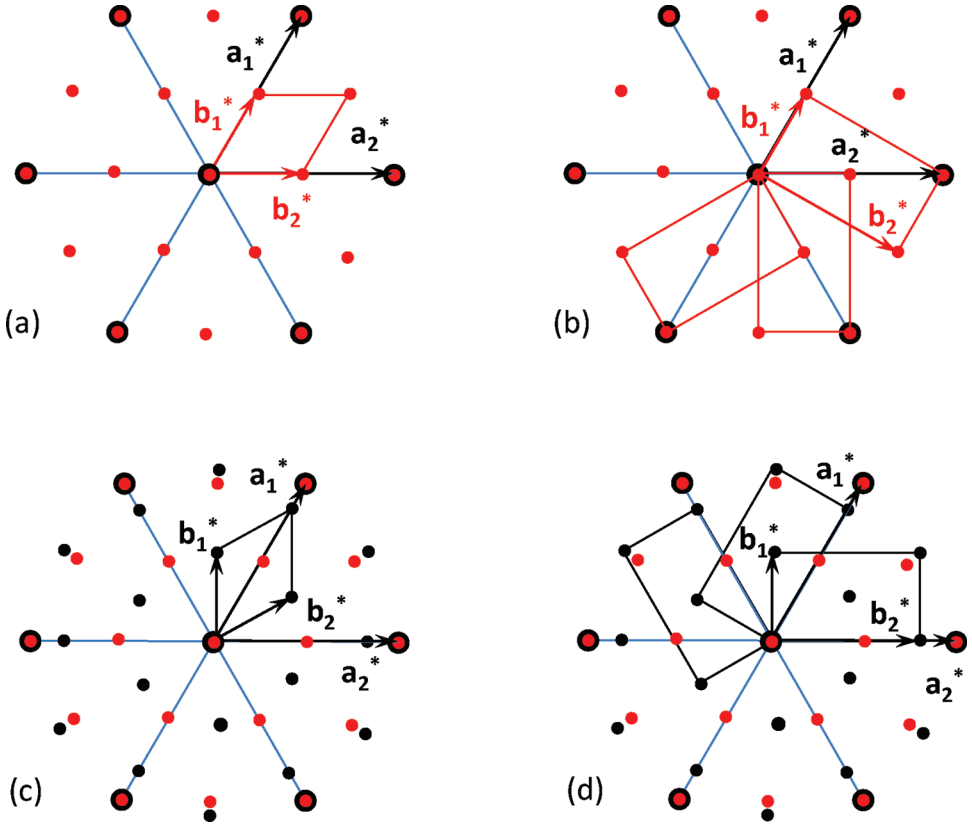

Figure 2. Diffraction spots associated with the LEED patterns given in Figure 1. (a) (2 × 2) superstructure (red spots), (b) (1 × 2) superstructures (red spots), (c) (2 × 2)R30° superstructure (black spots), and (d) (1 × 2)R30° domains superstructures (black spots). Substrate and overlayer unit cell vectors are denoted with a_1^*/a_2^* and b_1^*/b_2^*, respectively. The big black spots correspond to the diffraction spots of the Pt(111) substrate surface.

signal via the following equation[21]

$$d_{ox} = \lambda \sin\theta \ln[((I_{Pt}^{\infty} - I_{Pt})/I_{Pt}) + 1] \quad (1)$$

where λ is the inelastic mean free path of the photoelectrons in the oxide film determined via QUASES-IMFP-TPP2M ver 2.2 software, $\theta = 48°$ is the take-off angle between the surface plane and the outgoing photoelectrons, I_{Pt}^{∞} is the intensity of the $Pt4f_{7/2}$ signal for a clean Pt(111) surface, and I_{Pt} is the intensity of the $Pt4f_{7/2}$ signal for the BaO_x/Pt(111) surface. In the coverage calculations, BaO_x monolayer thickness was assumed to be 0.39 nm, corresponding to the interlayer spacing in the ⟨110⟩ direction of the bulk BaO unit cell.

3. RESULTS AND DISCUSSION

3.1. Structure of BaO_x Overlayers on Pt(111). The long-range ordering of the BaO_x overlayers on Pt(111) as a function of BaO_x surface coverage was investigated using LEED. Figure 1 presents LEED patterns obtained for a clean Pt(111) surface (Figure 1a) and a BaO_x(0.5 MLE)/Pt(111) surface (Figure 1b–f). Ba evaporation on a Pt(111) substrate precovered with NO_2/N_2O_4 multilayer at 100 K and subsequent heating in vacuum to 300 K yield the LEED pattern in Figure 1b, revealing additional diffuse LEED spots with a (2 × 2) structure. Note that at this temperature the surface still contains various strongly bound NO_x species in the form of nitrates and nitrites, as will be discussed further in the later sections. Flash heating this surface in vacuum at 1073 K removes all NO_x species and reveals the LEED image given in Figure 1c, where the (2 × 2) spots become more apparent together with a new set of poorly defined diffraction spots. Annealing this surface at 1073 K for 20 min reveals the LEED pattern given in Figure 1d. Along with a (2 × 2) structure, formation of a (2 × 2)R30° structure with weak and diffuse diffraction spots are also visible. These weak (2 × 2)R30° spots become stronger upon an additional annealing in vacuum at 1073 K for 40 min (Figure 1e). Final annealing of the surface given in Figure 1e at 1073 K in vacuum for 60 min leads to the disappearance of the (2 × 2)R30° structure while the (2 × 2) spots becomes sharper (Figure 1f). The unit cells corresponding to the LEED patterns in Figure 1b,f are shown in Figure 2, where both of these LEED patterns are explained by the presence of a single (2 × 2) overlayer (Figure 2a) or the presence of multiple (1 × 2) overlayer domains that are rotated by 60° with respect to each other (Figure 2b). The LEED patterns given in Figure 1c–e can be explained by the presence of (2 × 2) (Figure 2a) or (1 × 2) overlayer structures (Figure 2b) and the presence of a coexisting (2 × 2)R30° overlayer structure (Figure 2c) or multiple (1 × 2)R30° domains that are rotated by 60° with respect to each other (Figure 2d).

Ordered BaO_x overlayers on Pt(111) were also observed for higher BaO_x surface coverages such as θ_{BaOx} = 1.5 MLE. The LEED pattern obtained for a BaO_x (1.5 MLE)/Pt(111) surface presenting a long-range order is shown in Figure 3a. This rather complicated LEED pattern can be analyzed by considering the superposition of three different rectangular BaO_x overlayer domains coexisting on the Pt(111) substrate that are rotated with respect to each other by 60° (Figure 3b). These overlayer

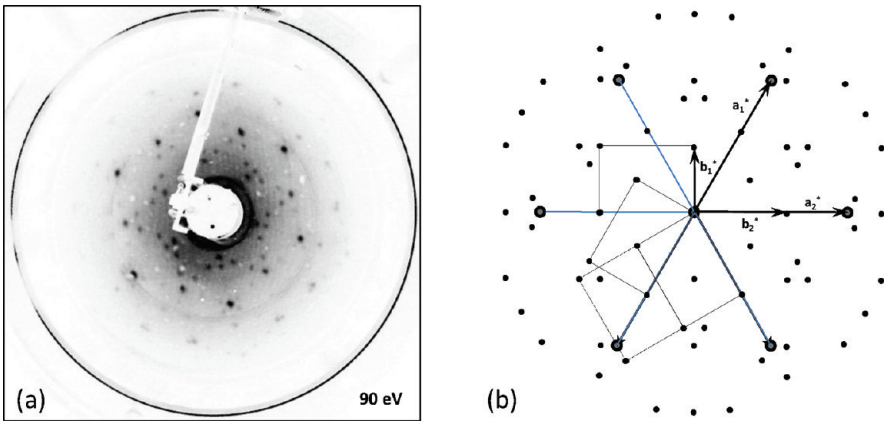

Figure 3. (a) Representative LEED pattern of an ordered BaO_x(1.5 MLE)/Pt(111) film and (b) schematic showing the unit cell structure associated with this LEED pattern. Substrate and overlayer unit cell vectors are denoted with a_1^*/a_2^* and b_1^*/b_2^*, respectively. The big black spots correspond to the Pt(111) substrate surface.

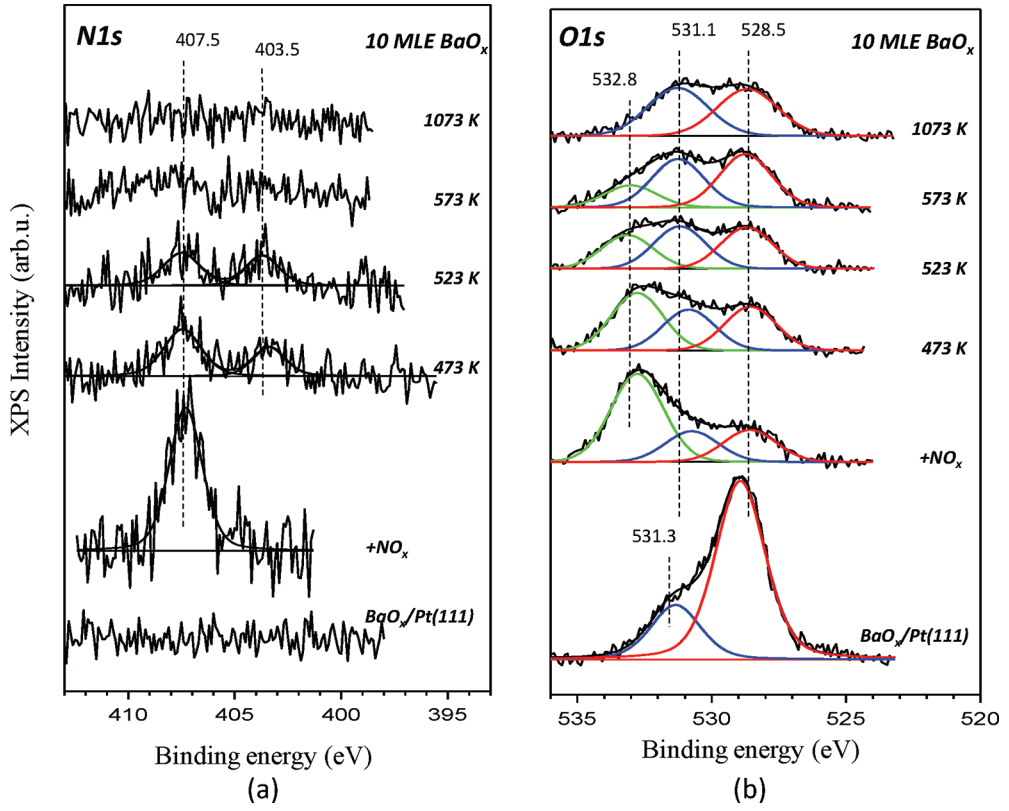

Figure 4. N1s (a) and O1s (b) XPS core level spectra for BaO_x(10 MLE)/Pt(111) exposed to 3600 L (10^{-6} Torr × 60 min) NO_2 at 323 K and the XP spectra obtained after subsequent annealing steps in vacuum performed at 473, 523, 573, and 1073 K.

domains that comprise the major portion of the observed spots possess a unit cell defined by 3.9 × 5.5 Å^2 rectangles in real space, although the presence of other coexisting ordered domains cannot be ruled out. The bulk BaO has a cubic *Fm*3*m* structure with a_0 = 5.53 Å, and the observed 3.9 × 5.5 Å^2 rectangular structure for the BaO_x (1.5 MLE)/Pt(111) surface indicates that this surface exhibits BaO(110) facets. The 5.5 Å interatomic distance in BaO(110) surface structure is almost twice the Pt−Pt distance (2.77 Å) in Pt(111), which may facilitate the formation of the BaO(110) ordered overlayer. It is worth mentioning that BaO_x/Pt(111) surfaces with θ_{BaOx} > 2.5 MLE did not reveal any long-range order and were found to be amorphous.

BaO overlayers exhibiting long-range order were also reported in former studies. For instance, the formation of a BaO (100) overlayer structure was observed on Cu (111) using LEED.[18] BaO (100) surface plane of bulk BaO unit cell has the lowest surface free energy compared with other surface facets.[20] Therefore, the formation of the BaO(100) surface is not surprising when the support has limited influence on the BaO overlayer due to an epitaxial mismatch leading to a weak interaction between

the substrate and the overlayer. The structure of the BaO overlayers on the Pt(111) substrate has been previously investigated by STM for a relatively high BaO coverage of 3 ML, where no well-defined structure could be detected in LEED.[12,19] In these STM studies, a hexagonal BaO structure with an atomic spacing of 8.1 Å was observed, which was accounted for by the presence of a (2×2) reconstructed BaO(111) surface. It is worth mentioning that the currently observed BaO(110) and $(2 \times 2)/(1 \times 2)$ BaO/Pt(111) ordered overlayer structures had not been previously reported.

3.2. NO_2 Adsorption on Thick BaO_x Overlayers on Pt(111). To avoid the influence of the exposed Pt(111) sites (i.e., Pt sites that are not covered by BaO_x domains) on the NO_x storage and release properties of BaO_x domains, we first performed NO_2 adsorption experiments on a model catalyst having a relatively thick BaO_x overlayer (i.e., BaO_x(10 MLE)/Pt(111)). Figure 4 summarizes the XPS measurements obtained for the saturation of such a surface with NO_2 at 323 K, followed by stepwise thermal NO_x desorption at various temperatures in vacuum.

The bottommost spectrum in Figure 4a shows the N1s region of the XP spectrum for the freshly prepared BaO_x(10 MLE)/Pt(111) sample. After an NO_2 exposure of 3600 L ($P_{NO_2} = 10^{-6}$ Torr $\times$ 60 min, 1 L = 10^{-6} Torr·s) at 323 K, a relatively strong peak becomes visible at 407.4 eV (Figure 4a, spectrum labeled with "+NO_x"), which can be assigned to nitrate (NO_3^-) species.[10,22] Nitrite (NO_2^-) species that have a characteristic peak at ~404 eV[23] are not readily visible in this spectrum (although a minor contribution from such species cannot be excluded). In the previous investigations[5,10] of NO_2 adsorption on BaO/Pt(111) system at 300 K, it has been shown that during the initial stages of NO_2 adsorption, nitrite formation precedes the formation of nitrates, whereas increasingly large exposures of NO_2 lead to the conversion of nitrite species into nitrates on the surface. Therefore, the NO_2 exposure used in the current study corresponds to a BaO_x(10 MLE)/Pt(111) surface that is almost saturated with NO_x in which nitrate species are the predominant NO_x species on the model catalyst surface. Annealing this surface at 473 K in vacuum results in the attenuation of the nitrate signal in XPS (Figure 4a) and the formation of a new N1s signal at 403.5 eV, which can be ascribed to nitrite species.[24,25] Observation of nitrite species during the thermal decomposition of nitrates suggests that the nitrate release mechanism from the BaO_x(10 MLE)/Pt(111) model catalyst surface involves nitrite species. This can be mechanistically envisaged by considering the reaction pathway given below

$$Ba(NO_3)_2 \rightarrow Ba(NO_2)_2 + O_2 \quad (2)$$

$$Ba(NO_3)_2 + 2BaO \rightarrow Ba(NO_2)_2 + 2BaO_2 \quad (3)$$

$$Ba(NO_2)_2 \rightarrow BaO_2 + 2NO \quad (4)$$

$$2BaO_2 \rightarrow 2BaO + O_2 \quad (5)$$

However, a direct nitrate decomposition route cannot be excluded, which may operate simultaneously with the nitrite pathway

$$Ba(NO_3)_2 \rightarrow BaO_2 + 2NO + O_2 \quad (6)$$

$$Ba(NO_3)_2 + 2BaO \rightarrow 3BaO_2 + 2NO \quad (7)$$

It is seen in Figure 4a that above 573 K, the entire N1s signal in XPS vanishes. It is worth mentioning that although N 1s signal intensity goes below the detection limit of the currently utilized XPS electron energy analyzer at 573 K (which is also partially due to the small photoemission cross sections of N1s species), under these conditions, the BaO_x(10 MLE)/Pt(111) surface is not free of NO_x species, as verified by the O 1s XPS and TPD data discussed below.

The O1s region of the XP spectrum corresponding to a freshly prepared BaO_x(10 MLE)/Pt(111) surface is given at the bottom of Figure 4b. Two major features are visible in this spectrum, located at 528.9 and 531.1 eV. The former feature is attributed to BaO species in previous studies,[5,10,18] whereas the latter one can be tentatively assigned to BaO_2.[8,11] It should be mentioned that the 531.1 eV feature may also be attributed (at least in part) to O1s features associated with carbonate or hydroxyl species. We believe that although the contribution of carbonate or hydroxyl species to this peak cannot be completely excluded, their contribution should not be significant either. First, Figure 4b clearly indicates that the intensity of the 531.1 eV feature remains rather intact even after thermal annealing steps in vacuum at elevated temperatures such as 523−1073 K, which are well above the typical decomposition temperatures of barium carbonates and barium hydroxides. This argument is also supported by our current TPD data in which m/z = 18 and 44 were also monitored in a routine fashion. These results reveal a characteristically small m/z = 18 desorption signal located at T < 600 K (due to the decomposition of −OH species) and another minor m/z = 44 signal at T < 850 K (due to the decomposition of $-CO_3$ species). This suggests that if the 531.1 eV feature had had a major contribution from carbonate or hydroxyl species, then the intensity of this peak would have decreased by a considerable extent after thermal treatment at 1073 K, which obviously is not the case in Figure 4b. After the NO_2 exposure on this surface at 323 K, a very strong feature becomes visible at 532.8 eV, which is associated with the nitrate/nitrite species.[5,8] Annealing at 473 K leads to attenuation of the signal at 532.8 eV due to the partial decomposition of nitrates/nitrites and NO_x release from the surface. After the annealing step at 573 K, a significant fraction (but not all) of the O1s signal associated with NO_x species is lost. This indicates that the BaO_x(10 MLE)/Pt(111) surface still contains some thermally stable ionic NO_x species under these conditions. Finally, annealing at 1073 K gives rise to the complete disappearance of the O1s signal associated with NO_x species. An important observation for the O1s spectra presented in Figure 4b is the growth of the 531 eV (BaO_2) feature during the thermal NO_x decomposition/desorption at elevated temperatures, suggesting the fact that $Ba(NO_x)_2$ decomposition is accompanied by the BaO_2 formation. These BaO_2 species exhibit a high thermal stability, as seen from the intense 531 eV signal that is present even after annealing at 1073 K. It is worth mentioning that analogous experiments performed on BaO_x(5 MLE)/Pt(111) revealed that the NO_x uptake and release behavior of these BaO_x overlayers are rather similar to the BaO_x(10 MLE)/Pt(111) model catalyst. It should be also noted that as-deposited metallic Ba overlayers on the Pt(111) substrate in the absence of externally introduced oxidizing agents such as O_2 or NO_2 reveal a typical $Ba3d_{5/2}$ binding energy (BE) of ~780.9 eV (data not shown). Oxidized BaO_x overlayers on Pt(111) exhibit a typical $Ba3d_{5/2}$ signal that is shifted to 779.3−779.8 eV, depending on the BaO_x surface coverage. The origin of this well-known negative BE shift observed during the oxidation of metallic Ba species has been thoroughly discussed in our previous reports as well as in other former studies in the literature.[10,25]

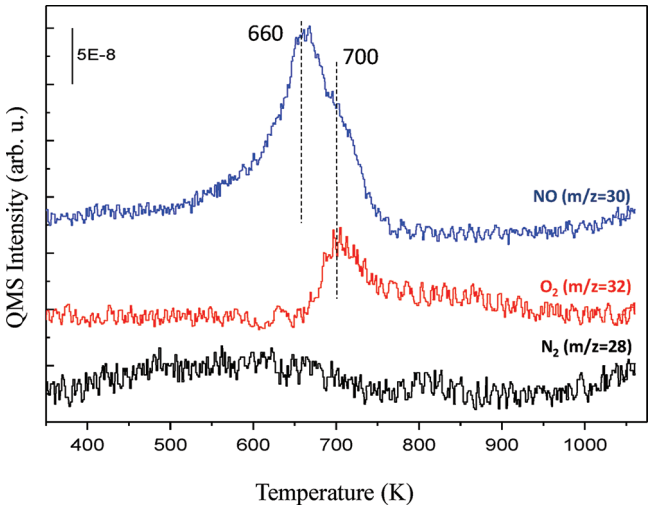

Figure 5. TPD spectra for the NO ($m/z = 30$), O_2 ($m/z = 32$), and N_2/CO ($m/z = 28$) channels obtained after exposing the BaO_x(10 MLE)/Pt(111) surface to 900 L (5×10^{-7} Torr $\times$ 30 min) NO_2(g) at 323 K.

Figure 5 presents the TPD spectra acquired after 900 L (5×10^{-7} Torr $\times$ 30 min) NO_2 exposure on a freshly prepared BaO_x(10 MLE)/Pt(111) model catalyst surface at 323 K. Two major NO desorption features at 660 and 700 K are evident in the $m/z = 30$ channel in Figure 5 with a weak low-temperature shoulder within 450−600 K. O_2 ($m/z = 32$) desorption signal reveals an asymmetric peak at 700 K with a high-temperature tail extending up to 950 K. The N_2 desorption channel ($m/z = 28$) presents a very weak and poorly defined signal, suggesting the lack of a significant amount of N_2 evolution.

The low-temperature NO desorption shoulder located within 450−600 K in Figure 5 can be assigned to nitrate/nitrite decomposition over small BaO_x clusters. This assignment is in very good agreement with the current BaO_x coverage-dependent TPD experiments that are described below as well as with other former studies given in the literature suggesting that "surface" nitrate decomposition occurs at a much lower temperature (i.e., 450−600 K) on the small BaO_x clusters due to the lack of stable "bulk" $Ba(NO_3)_2$ species.[26] The main NO desorption signal displays two characteristically different pathways for $Ba(NO_3)_2$ decomposition. The first decomposition pathway proceeds at 660 K via only NO(g) desorption (i.e., without any O_2 evolution). This first pathway can be envisaged with the help of reactions 3, 4, and 7 given above. In this first decomposition pathway, presumably O(ads) species generated due to the nitrate/nitrite decomposition diffuse on the $BaO_x/Ba(NO_x)_2$ surface and oxidize the BaO domains in the close proximity of the reaction center to form BaO_2 (as verified by the current XPS results given in Figure 4b). Furthermore, some of these O(ads) species may also diffuse into the subsurface region or titrate some oxygen-deficient point defect sites, before they get a chance to recombinatively desorb as O_2(g). Once the surface/subsurface region is saturated with oxygen and the BaO_2 formation process halts, the second decomposition pathway starts to operate at 725 K, which leads to the desorption of NO(g) + O_2(g). This second pathway can be envisaged through the chemical reactions 2, 4, and 6 given above. Furthermore, the high-temperature O_2 desorption tail visible at 800−900 K can be ascribed to the oxygen evolution due to the partial decomposition of BaO_2 species into BaO. Note that a significant fraction of BaO_2 species manages to exist on the surface even after annealing at 1073 K, as shown in Figure 4b. In a former study on NO_2 adsorption on BaO/Pt(111) system,[7] a similar two-stage NO_x desorption behavior was observed where in the first stage NO_2(g) + NO (g) release was monitored at 596 K, followed by a second desorption stage yielding NO(g) + O_2(g) evolution at 670 K. This previously observed two-stage mechanism was attributed to the presence of different types of nitrate species; however, even vibration spectroscopy was not able to verify conclusively the presence of two distinct types of nitrate species. Therefore, it is plausible that the currently suggested two-stage NO_x decomposition mechanism involving the formation and partial decomposition of BaO_2 species provides either an alternative or a complementary explanation for the fundamental surface scientific phenomena, which is crucial for the molecular understanding of the NO_x storage process in NSR systems. In contrast with the former results in the literature[7] where a small but a detectable amount of NO_2 desorption was observed, our TPD results do not show any detectable NO_2 ($m/z = 46$) desorption signal. This could be due to the particular design of the QMS shield used in the current TPD experimental setup that might have a larger dead volume between the sample and the QMS ionization compartment enabling the already small number of NO_2 molecules desorbing from the sample to make multiple collisions with the walls of the QMS shield yielding NO(g) + 1/2O_2(g) or NO(g) + O(ads). Furthermore, it is well known that the quantitative detection of NO_2(g) in UHV systems via conventional electron impact ionization QMS instrumentation is rather problematic because of the self-decomposition of NO_2 in the gas phase and the facile fragmentation of the NO_2 into NO and O_2 in the ionization compartment of the QMS (which also strongly depends on the QMS instrumentation parameters such as electron acceleration potential and the filament emission current) yielding a typical ($m/z = 30$)/($m/z = 46$) signal ratio of ~3/1. Furthermore, in the TPD experiment given in Figure 5, N_2O/CO_2 ($m/z = 44$) desorption channel was also simultaneously monitored (data not shown) along with other desorption channels. A broad and a weak $m/z = 44$ signal was detected with a desorption maximum at ~800 K. This peak was attributed to the CO_2 desorption due to background CO/CO_2 adsorption (at ~5×10^{-10} Torr) resulting in the formation of strongly bound carbonate species that decompose at 800 K. Such a CO_2 desorption signal originated from background species was also reported for similar surfaces in the literature.[7,18] To confirm this assignment, we performed a control ("blank") TPD experiment on a freshly prepared BaO_x/Pt(111) surface without introducing any adsorbates prior to the TPD run. This "blank" TPD experiment also yielded a weak $m/z = 44$ desorption signal at ~800 K, in accord with the current assignment.

3.3. Influence of the BaO_x Overlayer Growth Conditions on the Surface Composition, Morphology. and Reactivity of Thick BaO_x Films. As described above, currently exploited BaO_x overlayer growth methodology, which is also called the reactive layer assisted deposition or RLAD approach, utilizes the NO_2 multilayers as the oxidizing agent during the oxidation of the deposited metallic Ba species on the Pt(111) substrate. Several former studies in the literature used O_2 for the growth of similar metal oxide overlayers.[6,10,18] Therefore, we have also prepared BaO_x/Pt(111) model catalyst systems where O_2 was also used as an additional oxidizing agent. In this alternative preparation protocol, after Ba deposition onto the N_2O_4 multilayer on the

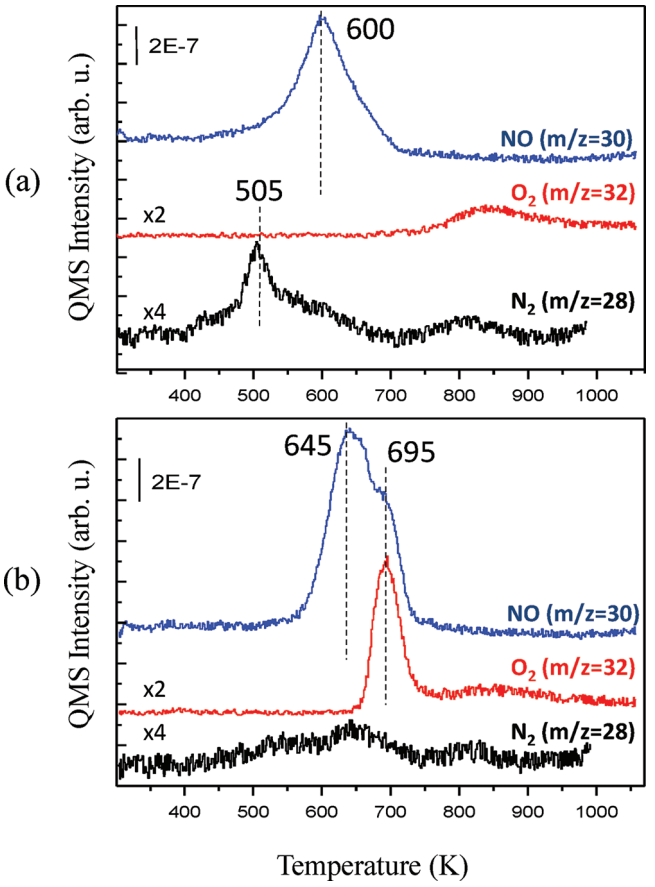

Figure 6. (a) TPD spectra for the NO ($m/z = 30$), O_2 ($m/z = 32$), and N_2/CO ($m/z = 28$) channels obtained after exposing a freshly prepared BaO_x(10 MLE)/Pt(111) surface to 900 L (5×10^{-7} Torr $\times$ 30 min) NO_2(g) at 323 K where the BaO_x overlayer was grown using an additional annealing step in O_2(g) (i.e., the second preparation procedure described in the text). (b) TPD spectra for the NO ($m/z = 30$), O_2 ($m/z = 32$), and N_2/CO ($m/z = 28$) channels obtained after exposing a BaO_x(10 MLE)/Pt(111) surface to 900 L (5×10^{-7} Torr $\times$ 30 min) NO_2(g) at 323 K, which is initially prepared by the second procedure given in the text and then subsequently treated with multiple NO_x uptake and release procedures prior to the TPD run. (See the text for details.)

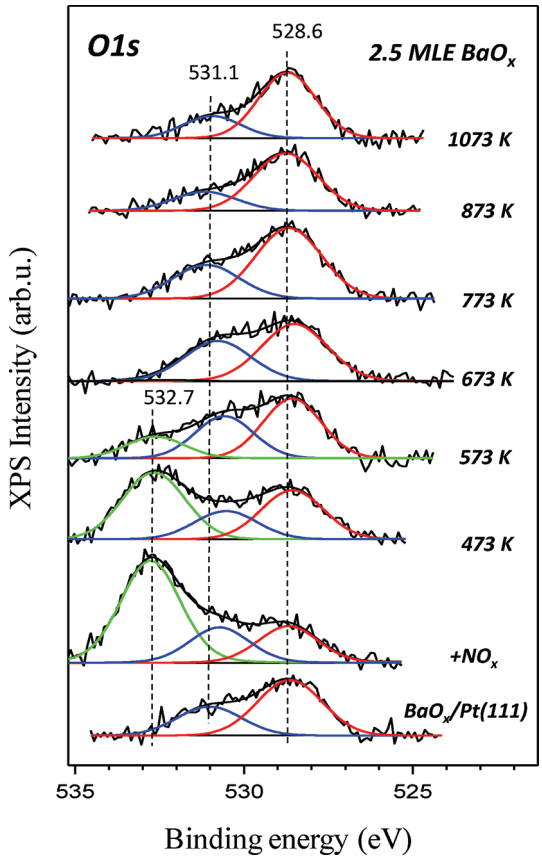

Figure 7. O1s XPS core level spectra for the BaO_x(2.5 MLE)/Pt(111) surface that is exposed to 900 L (5×10^{-7} Torr $\times$ 30 min) NO_2 at 323 K and after subsequent annealing steps in vacuum at the given temperatures.

Pt(111) substrate at 100 K, the sample was heated to 873 K in 10^{-7} Torr of O_2(g). (Note that throughout the text, unless mentioned otherwise, it should be assumed that the first preparation procedure was used for the growth of BaO_x overlayers on the Pt(111) substrate.)

A BaO_x(10 MLE)/Pt(111) model catalyst surface prepared via this (second) alternative synthetic protocol was then exposed to 900 L NO_2 ($P_{NO_2} = 5 \times 10^{-7}$ Torr $\times$ 30 min) at 323 K. XPS analysis of the N1s region (data not shown) indicated relatively similar types of NO_x species as in the case of the first preparation protocol. After the NO_2 adsorption on this surface, nitrates (characterized by a N1s signal at 407.5 eV) were the predominant NO_x species, whereas nitrites (characterized by a N1s signal at 403.5 eV) also existed on the surface to a lesser extent with a relative surface coverage of $NO_2^-/NO_3^- < 0.15$. The TPD spectra obtained for this surface after the NO_2 exposure are given in Figure 6a. The major NO desorption feature appears as an asymmetric peak at 600 K, which is not accompanied by O_2 evolution.

As previously described, the lack of O_2 desorption signal within 500−700 K can be explained by the formation of BaO_2 species and the diffusion of O(ads) into the subsurface region. It is worth emphasizing that the main NO desorption signal in Figure 6a is located at a noticeably lower temperature (i.e., 600 K) than the one given in Figure 5 (i.e., 660 K), implying a decrease in the thermal stability of the nitrate species. Recalling the two-stage NO_x decomposition mechanism discussed above, it can be argued that only one of these decomposition pathways operates in Figure 6a. This low-temperature nitrate/nitrite decomposition pathway is accompanied by BaO_2 formation, as verified by the corresponding O1s XPS data given in Figure 7. However an important difference in Figure 6a is that BaO_2 formation continues to occur all throughout the NO_x decomposition window, which is implied by the lack of O_2 signal within 500−700 K. Therefore, for the TPD data given in Figure 6a, there seems to be a unique structural factor facilitating the peroxide formation. In addition to these observations, the broad peak of O_2 desorption signal seen in Figure 6a at 750−1000 K can be associated with the decomposition of some (but not all) of the BaO_2 species on the surface.

The most striking aspect of Figure 6a is the observation of the readily visible $m/z = 28$ desorption signal at 505 K, accompanied by a minor desorption signal at 800 K. To elucidate the origin of these desorption signals, we performed a control "blank" experiment on a freshly prepared BaO_x(10 MLE)/Pt(111) surface via the second synthetic protocol in the absence of any additional

Scheme 1. Description of the Different Preparation Procedures Used for the Growth of BaO_x/Overlayers on the Pt(111) Substrate Surface

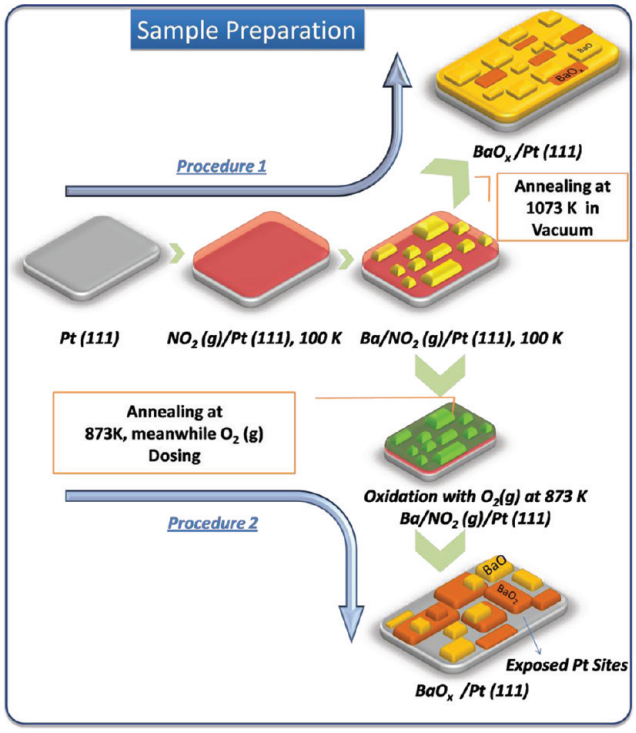

adsorbates (data not shown). This control experiment revealed only a weak m/z = 28 desorption signal at ~800 K, and no significant m/z = 28 desorption signal was detected within 400−600 K. In light of this control experiment, the 505 K feature in the m/z = 28 channel in Figure 6a can be attributed to N_2 desorption (occurring during the nitrate decomposition/release process), whereas the weak feature at 800 K is associated with CO desorption due to background CO adsorption and carbonate formation. Such an observation of N_2 evolution from a thick BaO_x overlayer is rather unexpected, as it is known that alkaline earth oxide surfaces such as BaO cannot efficiently activate N−O linkages and catalyze the formation of atomic N(ads) species that can recombinatively desorb as N_2.[27] It is well known that precious metal surfaces such as Pt(111) can catalyze N−O bond rupture yielding atomic N(ads) and O(ads) species.[28] It was suggested in a former report that the formation of N(ads) species on Pt(111) occurs on the surface defect sites revealing a N_2 desorption signal in TPD at 475 K with a broad tail within 500−750 K.[28] Therefore, the N_2 desorption signal in Figure 6a is attributed to the presence of exposed Pt sites on the BaO_x(10 MLE)/Pt(111) surface, which are generated because of the formation of BaO_2 species during the alternative film growth procedure (involving an additional high-temperature oxidation step in O_2). It is likely that the BaO_2−BaO overlayer has a distinctly different surface morphology and surface wetting characteristics on the Pt(111) substrate than that of the BaO overlayer, as shown in Scheme 1. The presence of exposed Pt sites is also in line with the lack of two-stage NO_x decomposition process in Figure 6a (i.e., suppression of the NO desorption signal at 650−700 K). As described above, the second stage of the nitrite/nitrate decomposition process (releasing NO + O_2) in Figure 5 starts only after the BaO_2 formation process halts, and the surface/subsurface region can no longer accommodate O(ads) species generated by the nitrate decomposition, probably due to the limited surface/bulk diffusion of O(ads) species on/in BaO_2 domains. Simultaneous desorption of NO and O_2 is not at all observed in Figure 6a, suggesting the continuous formation of BaO_2 species during the nitrate decomposition. This can be explained by the presence of exposed Pt sites that are in close proximity of the BaO−BaO_2 domains, which function as oxygen transporters facilitating the transfer/diffusion of O(ads) species toward BaO sites and catalyzing their oxidation to BaO_2.

An interesting aspect of the BaO_x(10 MLE)/Pt(111) surfaces with exposed Pt surface sites is their ability to be "cured". In other words, the exposed Pt surface sites in these systems can be covered back with BaO/BaO_2 domains. We found out that this morphological curing effect can be achieved by successive NO_2 adsorption and thermal desorption cycles. Figure 6b presents TPD spectra obtained after NO_2 adsorption on a BaO_x(10 MLE)/Pt(111) surface prepared via an additional O_2 oxidation treatment, followed by seven subsequent nitration-thermal desorption cycles. The general characteristics of the TPD traces given in Figure 6b strongly resemble the TPD data given in Figure 5. Reappearance of the two-stage NO_x decomposition process and the suppression of the N_2 desorption imply that the BaO-BaO_2 domains rewet the Pt(111) substrate surface covering the exposed Pt(111) sites. Therefore, it is apparent that the morphological transformations of the BaO_x overlayers on Pt(111) are rather reversible where the "wetting/dewetting" of the overlayer can be controlled by varying the oxidation conditions.

3.4. NO_2 Adsorption on thin BaO_x Overlayers on Pt(111). The bottommost O1s XP spectrum in Figure 7 demonstrates the XPS data obtained for a fresh BaO_x(2.5 MLE)/Pt(111) surface prepared by the first protocol (i.e., without an additional oxidation step in O_2) revealing the existence of both BaO (528.6 eV) and BaO_2 (530.8 to 531.1 eV) species. The spectrum in Figure 7 labeled with "+NO_x" was acquired after exposing 900 L (5×10^{-7} Torr × 30 min) NO_2 on this surface at 323 K, indicating the formation of nitrate/nitrite species (532.7 eV), which gradually decompose at higher temperatures and completely vanish above 673 K. It should be noted that the variations in the O1s BE values for the BaO_2 species within 530.6 to 531.2 eV might be associated with differential charging between BaO and BaO_2 domains. Alternatively, such BE shifts may also originate due to the existence of minor quantities of $BaCO_3$, $Ba(OH)_2$ species, or both (formed due to residual CO or H_2O adsorption from the background), which overlap with BaO_2 O1s feature and shift the final peak positions to higher BE values. Note that O1s BE values for $BaCO_3$ and $Ba(OH)_2$ are located at 531.5 eV[7] and 531.0−531.4 eV,[29] respectively. According to corresponding N1s spectra, nitrate thermal decomposition occurs with nitrite formation with total disappearance of N1s peaks after heating to 625 K (spectra are not shown). This N1s region behavior is quite similar to that observed for BaO_x(10 MLE)/Pt(111) overlayer in Figure 4a.

Comparison of the topmost O1s XP spectra given in Figure 4a, corresponding to relatively thick (10 MLE) BaO_x overlayers and Figure 7, corresponding to a thinner (2.5 MLE) BaO_x overlayer, reveals an important difference. It is apparent that the BaO_2/BaO O1s intensity ratio is much smaller at elevated temperatures for the thinner BaO_x overlayers, suggesting that the BaO_2 species that are formed on thinner BaO_x overlayers are thermally less stable. This can possibly be due to a stronger and a more direct

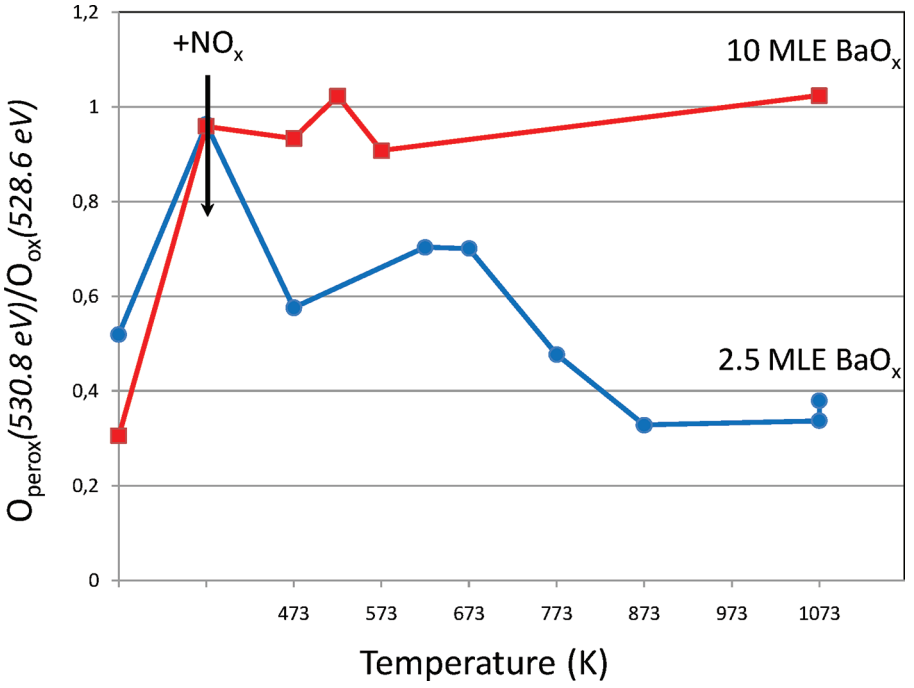

Figure 8. Plot showing the integrated O1s signal intensity ratios for O_{perox}(530.8 eV) and O_{ox}(528.6 eV) signals corresponding to the BaO_x(10 MLE)/Pt(111) surface (red squares) and BaO_x(2.5 MLE)/Pt(111) surface (blue circles) measured after nitration and subsequent stepwise heating.

interaction between the surface BaO_2 domains and Pt(111) sites, which can catalyze/facilitate the BaO_2 decomposition. Such a direct and strong interaction between BaO_2 species and the Pt(111) sites might be hindered in thicker films due to the lack of a direct physical contact between these two species. Alternatively, the decrease in the peroxide thermal stability for thin BaO_x overlayers can also be associated with the presence of cracks/holes in the BaO_x thin film that can lead to an increased number of exposed Pt-BaO_2 interfacial sites. The relative stability of BaO_2 species for BaO_x(2.5 MLE)/Pt(111) and BaO_x(10 MLE)/Pt-(111) surfaces at various temperatures are shown in Figure 8, where O_{perox}/O_{ox} atomic ratio values (derived from the XPS data given in Figures 4a and 7) are plotted as a function of temperature. It is clearly seen in Figure 8 that although BaO_2 species are rather stable for thick BaO_x even at elevated temperatures, the peroxide species on thinner BaO_x films readily decompose at elevated temperatures.

To investigate the influence of the BaO_x coverage on the NO_x storage/release behavior of model NSR catalysts in detail, we prepared BaO_x/Pt(111) model catalysts using the typical RLAD method described above (i.e., without performing annealing in O_2) with θ_{BaOx} = 0, 0.5, 0.8, 1.0, 2.5, 5.5, and 10 MLE. Then, each of these freshly prepared surfaces was exposed to 900 L ($P_{NO_2} = 5 \times 10^{-7}$ Torr × 30 min) at 323 K (except the θ_{BaOx} = 10 MLE case where the surface was exposed to 3600 L ($P_{NO2} = 10^{-6}$ Torr × 60 min)), and the TPD experiments were performed (Figure 9). Figure 9 clearly demonstrates the significant differences in the NO_x desorption characteristics of thin BaO_x overlayers (i.e., $\theta_{BaOx} \leq$ 1MLE) in comparison with the thicker ones (i.e., $\theta_{BaOx} \geq$ 2.5 MLE). The NO_x desorption behavior of the thicker films ($\theta_{BaOx} \geq$ 2.5 MLE) exhibits the usual two-stage NO_x decomposition character within 650−700 K, as described above. It is worth mentioning that N_2 and O_2 desorption signals for $\theta_{BaOx} \geq$ 2.5 MLE present a similar behavior as that of Figure 5 corresponding to relatively thick films lacking exposed Pt-sites. However, for the thin BaO_x overlayers (i.e., $\theta_{BaOx} \leq$ 1MLE), NO_x desorption temperatures present a drastic shift toward lower temperatures (375−460 K), and the desorption signal shifts further toward lower temperatures (333 K) for the clean Pt(111) surface (i.e., in the absence of BaO_x). For 1.0 and 0.8 MLE BaO_x coverages, two major desorption features appear at 415 and 460 K. The N_2 and O_2 desorption spectra for $\theta_{BaOx} \leq$ 1MLE reveal significant resemblances to the TPD data presented in Figure 6a that correspond to BaO_x/Pt(111) surface exhibiting exposed Pt sites. Taking into account the fact that the BaO_x overlayers at these low coverages are probably composed of mostly 2D islands in addition to small 3D clusters, it can be argued that the NO desorption signal at 415 K is associated with the nitrate/nitrite species located at the peripheral Pt-BaO_x interface sites of the 2D islands or small 3D clusters, where the NO_x decomposition process is assisted by the exposed Pt sites, whereas the 460 K feature is associated with the nitrate/nitrite decomposition on the terraces of 2D islands or the 3D clusters, which are farther away from the exposed Pt sites. Along these lines, it is likely that a large portion of the 375 K signal for the BaO_x (0.5 MLE)/Pt(111) surface can originate from NO_x decomposition directly on the exposed Pt(111) sites, whereas the high-temperature tail that is visible for BaO_x (0.8−1.0 MLE)/Pt(111) surfaces between 500 and 600 K may arise from the NO_x evolution from larger 3D clusters that reveal a bulk-like behavior, as observed for $\theta_{BaOx} \geq$ 2.5 MLE.

In a large number of former studies on realistic NSR catalysts in the literature, the influence of the so-called "surface nitrates" (i.e., nitrates stored on small 2D BaO agglomerates) and "bulk nitrates" (i.e., nitrates stored on or inside the large 3D BaO nanoparticles forming a $Ba(NO_3)_2$ shell and a BaO core structure) were extensively discussed. From this respect, Figure 9 demonstrates the influence of two important factors on the thermal stability of stored NO_x species, namely, BaO_x

dx.doi.org/10.1021/jp208269x |J. Phys. Chem. C 2011, 115, 24256–24266

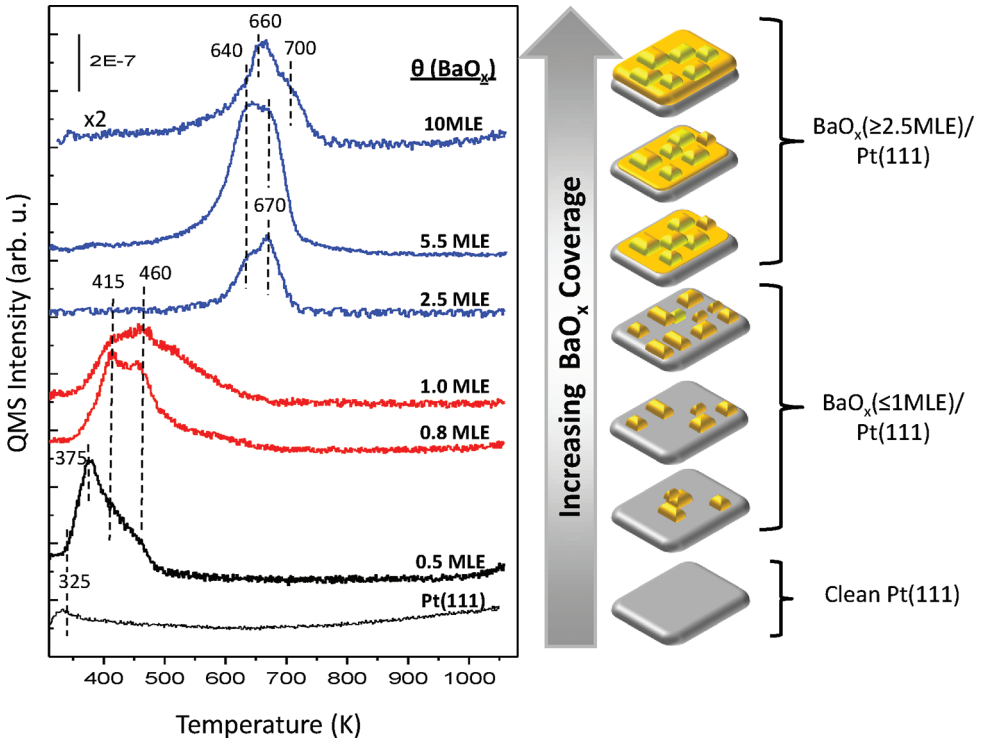

Figure 9. NO ($m/z = 30$) channel of the TPD spectra obtained after saturation of BaO_x/Pt(111) surfaces having different BaO_x surface coverages with NO_2 at 323 K.

domain/particle size and the presence of Pt/BaO_x interfacial sites. It is seen that decreasing the BaO_x domain/particle size and increasing the number of Pt/BaO_x interfacial sites decreases the desorption temperature of the stored NO_x species. In other words, the TPD results given in Figure 9 are particularly valuable because they provide a direct fundamental surface scientific evidence of the differences in the NO_x release properties of "surface" versus "bulk" BaO_x domains as well as the catalytic role of the exposed Pt sites that are in close proximity of the NO_x storage domains in NSR catalysts.

4. CONCLUSIONS

The surface structure and the NO_x storage/release properties of BaO_x/Pt(111) model catalyst were studied for a various BaO_x surface coverages prepared via different overlayer growth protocols. Our results can be summarized as follows:

- For $\theta_{BaOx} < 1$ MLE, (2×2) or (1×2) overlayer structures were determined via LEED, which exist simultaneously with metastable (2×2)R30° or (1×2)R30° overlayer structures, whereas for $\theta_{BaOx} = 1.5$ MLE, BaO(110) surface was found to exist. BaO_x/Pt(111) surfaces with $\theta_{BaOx} \geq 2.5$ MLE were found to be amorphous without any discernible LEED pattern.
- Extensive NO_2 exposure on the BaO_x(10 MLE)/Pt(111) surface at 323 K revealed the presence of mostly nitrates on the surface. Thermal decomposition of the stored NO_x species occurs in a two-stage mechanism, where in the first stage at ~650 K nitrite/nitrate species decompose into NO(g) + O(ads) resulting in the formation of BaO_2 without O_2(g) evolution, whereas in the second stage, NO(g) + O_2(g) evolution is observed at ~700 K.
- BaO_x overlayer preparation method has a strong influence on the morphology of the BaO_x domains. Preparation of the BaO_x(10 MLE)/Pt(111) surfaces with a typical RLAD method using NO_2 as an oxidant yields an overlayer that wets the Pt(111) substrate surface while an additional oxidation step involving O_2(g) leads to the extensive BaO_2 formation and dewetting. BaO_x(10 MLE)/Pt(111) surfaces prepared via this second protocol exhibit exposed Pt(111) sites that result in (a) enhanced BaO_2 formation, (b) a decrease in the thermal stability of the adsorbed nitrate species, and (c) catalytic activation of the N−O linkages and the formation of N(ads) species, which recombinatively desorb as N_2(g). Observed morphological changes of the BaO_x overlayers on the Pt(111) substrate (i.e., wetting/dewetting) were found to be reversible.
- BaO_x/Pt(111) surfaces prepared by varying BaO_x coverage revealed two characteristically distinct NO_x release behavior for $\theta_{BaOx} \leq 1.0$ MLE and $\theta_{BaOx} \geq 2.5$ MLE. For $\theta_{BaOx} \leq 1.0$ MLE, NO_x release takes place within 375−460 K, whereas for $\theta_{BaOx} \geq 2.5$ MLE, it occurs at 650−700 K. These two different NO_x release characteristics observed for two different coverage regimes can be explained by the presence of 2D-BaO_x islands and small 3D-BaO_x clusters in the former case and the existence of larger 3D-BaO_x nanoparticles in the latter case. These results provide a direct fundamental surface scientific evidence for the NO_x uptake and release properties of the so-called "surface/bulk nitrates" in realistic NSR catalysts

AUTHOR INFORMATION

Corresponding Author

*E-mail: ozensoy@fen.bilkent.edu.tr.

■ ACKNOWLEDGMENT

We gratefully acknowledge the financial support from the Scientific and Technical Research Council of Turkey (TUBITAK) (project code: 107Y115). E.O. also acknowledges support from Turkish Academy of Sciences (TUBA) for the "*Outstanding Young Investigator*" grant. E.I.V. and V.I.B. acknowledge RFBR (Russia) nos. 09-03-91225-CTa and 10-03-00596-a projects for financial support.

■ REFERENCES

(1) Shelef, M. *Chem. Rev.* **1995**, *95*, 209–225.
(2) Miyoshi, N.; Matsumoto, S.; Katoh, K.; Tanaka, T.; Harada, J.; Takahashi, N.; Yokota, K.; Sugiura, M.; Kasahara, K. *SAE Int. J. Engines* **1995**, 19950809.
(3) Hepburn, J. S.; Thanasiu, E.; Dobson, D. A.; Watkins, W. L. *SAE Int. J. Engines* **1996**, 19962051.
(4) Fekete, N.; Kemmler, R.; Voigtlander, D.; Krutzsch, B.; Zimmer, E.; Wenninger, G.; Strehlau, W.; van den Tillaart, J. A. A.; Leyrer, J.; Lox, E. S.; Muller, W. *SAE Int. J. Engines* **1997**, 19970746.
(5) Schmitz, P.; Baird, R. *J. Phys. Chem. B* **2002**, *106*, 4172–4180.
(6) Ozensoy, E.; Peden, C. H. F.; Szanyi, J. *J. Catal.* **2006**, *243*, 149–157.
(7) Mudiyanselage, K.; Yi, C.-W.; Szanyi, J. *Langmuir* **2009**, *25*, 10820–10828.
(8) Yi, C.-W.; Kwak, J. H.; Szanyi, J. *J. Phys. Chem. C* **2007**, *111*, 15299–15305.
(9) Yi, C.-W.; Szanyi, J. *J. Phys. Chem. C* **2009**, *113*, 2134–2140.
(10) Desikusumastuti, A.; Happel, M.; Dumbuya, K.; Staudt, T.; Laurin, M.; Gottfried, J. M.; Steinruck, H.-P.; Libuda, J. *J. Phys. Chem. C* **2008**, *112*, 6477–6486.
(11) Bowker, M.; Cristofolini, M.; Hall, M.; Fourre, E.; Grillo, F.; McCormack, E.; Stone, P.; Ishii, M. *Top. Catal.* **2007**, *42*, 341–343.
(12) Stone, P.; Ishii, M.; Bowker, M. *Surf. Sci.* **2003**, *537*, 179–190.
(13) Massalimov, I. A.; Kireeva, M. S.; Sangalov, Yu. A. *Inorg. Mater.* **2002**, *38*, 363–366 and references therein..
(14) Liu, Z.; Anderson, J. A. *J. Catal.* **2004**, *224*, 18–27.
(15) James, D.; Fourre, E.; Ishii, M.; Bowker, M. *Appl. Catal., B* **2003**, *45*, 147–159.
(16) Poulston, S.; Rajaram, R. R. *Catal. Today* **2003**, *81*, 603–610.
(17) Mudiyanselage, K.; Weaver, J. F.; Szanyi, J. *J. Phys. Chem. C* **2011**, *115*, 5903–5909.
(18) Tsami, A.; Grillo, F.; Bowker, M.; Nix, R. M. *Surf. Sci.* **2006**, *600*, 3403–3418.
(19) Bowker, M.; Stone, P.; Smith, R.; Fourre, E.; Ishii, M.; Leeuw, N. H. *Surf. Sci.* **2006**, *600*, 1973–1981.
(20) Broqvist, P.; Gronbeck, H.; Panas, I. *Surf. Sci.* **2004**, *554*, 262–271.
(21) Alexander, M. R.; Thompson, G. E.; Zhou, X.; Beamson, G.; Fairley, N. *Surf. Interface Anal.* **2002**, *34*, 485–489.
(22) Ozensoy, E.; Peden, C. H. F.; Szanyi, J. *J. Catal.* **2006**, *243*, 149–157.
(23) Ozensoy, E.; Peden, C. H. F.; Szanyi, J. *J. Phys. Chem. B* **2005**, *109*, 15977–15984.
(24) Jacobi, K.; Astaldi, C.; Frick, B.; Geng, P. *Phys. Rev.B* **1987**, *36*, 3079–3085.
(25) Ozensoy, E.; Peden, C. H. F.; Szanyi, J. *J. Phys. Chem. B* **2006**, *110*, 17009–17014 and references therein..
(26) Szanyi, J.; Kwak, J. H.; Kim, D. H.; Burton, S. D.; Peden, C. H. F. *J. Phys. Chem. B* **2005**, *109*, 27–29.
(27) Roy, S.; Baiker, A. *Chem. Rev.* **2009**, *109*, 4054–4091.
(28) Gland, J. L.; Sexton, B. A. *Surf. Sci.* **1980**, *94*, 355–368.
(29) Verhoeven, J. A., Th.; Doveren, H. *Surf. Sci.* **1982**, *123*, 369–383.